A fully self-driven power management circuit based on cycles for maximized energy output strategy for universal triboelectric energy harvesting

Yida Xin[1,2,3], Taili Du[1,2], Haiying Du[2], Dianlong Shen[1,2], Jing Wang[2], Peiting Sun[1,2], Minyi Xu[1,2]**

[1] Dalian Key Laboratory of Marine Micro/Nano Energy and Self-powered Systems, Marine Engineering College, Dalian Maritime University, Dalian 116026, China;

[2] State Key Laboratory of Maritime Technology and Safety, Dalian 116026, China.

[3] College of Mechanical and Electronic Engineering, Dalian Minzu University, Dalian 116600, China;

* Address correspondence to dutaili@dlmu.edu.cn; xuminyi@dlmu.edu.cn

Abstract

The inherent capacitor characteristic of the triboelectric nanogenerator (TENG) raises a significant challenge in achieving high energy harvesting efficiency. Power management has been treated as one of the most promising way to address this problem. Different from management only by traditional rectifier bridge, passive power management is more in line with the actual scenario of energy harvesting since it can eliminate the dependence on an external power supply. In this work, it introduces an innovative passive power management circuit (PMC) that employs cycles for maximized energy output strategy (CMEO) and unidirectional LC oscillation. Simulation results show that the proposed PMC can shorten the charging time to a 47 μF capacitor by 88.3%, and increase the effective output power of 1 MΩ by 17.35 times. The influence of semiconductor on the performance of the PMC and the sources of energy loss are revealed by numerical analysis for energy transfer. Furthermore, the relationship between these losses and device selection is investigated through simulation and experiment, which contributes to improving the power management performance and expanding the range of available TENGs. Through optimizing device selection, the fabricated PMC is successfully applied to another 6.7 μW low-output TENG, which exhibits its excellent adaptable potential to various TENGs.

Keywords: Passive power management, Triboelectric nanogenerator, Energy harvesting, Cycles for maximized energy output

Introduction

With the development of Internet of Things (IoT) technology, an increasing number of sensors are required to facilitate the interconnection of people, machines and things. These widely distributed sensors are typically powered by batteries and cables. However, battery-powered sensors encounter challenges such as periodic replacement, environmental pollution, and inaccessibility of certain sensor nodes, while cable power supply entails a large workload and high costs. To address the problem, harvesting various energy from the environment to power sensors has become an attractive choice. The triboelectric nanogenerator (TENG) is a new mechanical energy harvesting method based on triboelectrification and electrostatic induction, which was first proposed by Zhonglin Wang [1]. As validated by numerous scholars, TENGs can harvest various types of mechanical energy [2-5], offering unique advantages in ocean energy harvesting [6-9], vibration energy harvesting [10-13], acoustic energy harvesting [14-18] and flexible wearable devices [19-21]. Therefore, TENGs are anticipated to provide a new solution to the power supply challenge faced by a large number of microelectronic devices.

Since the equivalent model of TENG can be viewed as a voltage source and capacitor in series, its output inherently exhibits the characteristics of high voltage, low current, and high impedance [22]. Power management can effectively improve the energy harvesting performance of TENGs, and thus become a research focus in recent years [23-27]. Relevant research can be divided into capacitive load and resistive load according to the type of external load [3, 28]. The power management strategy mainly includes the buck converter strategy [29, 30] and the CMEO strategy [31-33]. Nevertheless, due to the sophisticated conduction control of switches, previous reports on power management are employed by active controllers. This contradicts the typical scenario where no power source is available for energy harvesting. Therefore, the realization of passive power management is very important for the TENG's practical

application. Currently, the implementation of passive power management mainly includes the structural design method [34, 35] and the electronic device method [36]. The structural design method takes considerable effort in the structural design of TENGs, which lacks universality. The electronic device method controls the switch through circuits, which has the characteristics of simplicity and strong versatility. Notably, Harmon et al. [36] designed a passive PMC based on the buck converter strategy in 2020, which achieved an energy conversion efficiency of 84.3% at 2 MΩ resistor. However, as an important method of power management strategies, research on CMEO-based passive power management is rarely reported. Given that the energy output of a TENG per cycle in CMEO mode reaches the theoretical maximum, the CMEO-based passive PMC has more potential for performance improvement.

In this work, a passive CMEO-ULC PMC is proposed to enhance energy harvesting efficiency. It employs the CMEO strategy to maximize the output and effectively transfers energy through unidirectional LC oscillation. Simulation results show that the PMC can shorten the charging time of a 47 μF capacitor to 3V by 88.3% and increase the output power of 1 MΩ resistor by 17.35 times. Since the performance of the PMC is susceptible to devices, the impact study of devices on the power management performance is conducted thoroughly. By establishing the numerical equation of the energy transfer process, energy loss sources are first identified. Then, the relationships between these losses and devices are analyzed. Through optimizing device selection, the energy loss of the PMC can be reduced effectively. With the help of the PMC, the experiment demonstrates that a 6.7 μW output TENG's charging time can be shortened by 62.8% and its output power of 1 MΩ is increased by 3.48 times. Additionally, the PMC also exhibits good versatility to various TENGs.

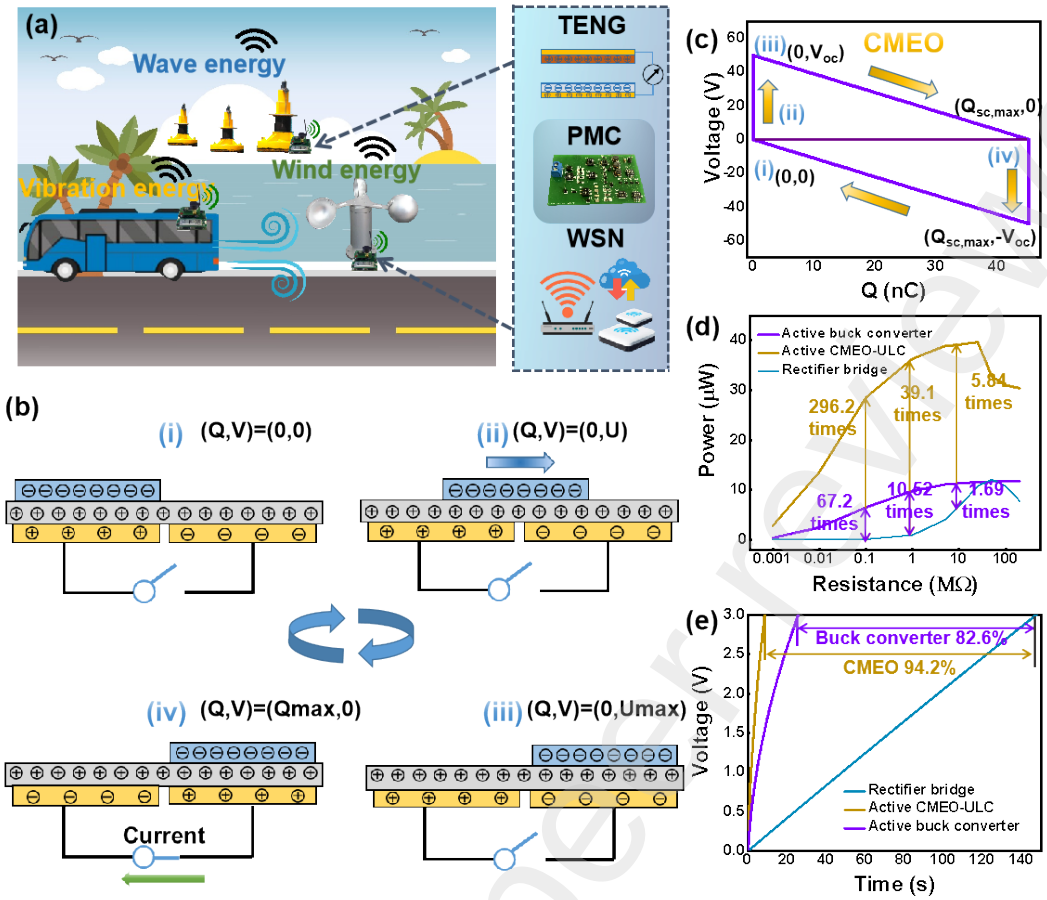

Fig. 1. Schematic illustration of the power management strategy. (a) Schematic illustration of TENG-based wireless sensor operation in the IoTs. (b) Working principle, and (c) V-Q diagram of the CMEO strategy. (d) Comparison of the output power, and (e) the charging performance between different active power management strategies.

2. Passive power management circuit

2.1 Power management strategy

TENGs can harvest various mechanical energy from the environment, such as vibration, wave and wind, which makes it a promising solution to power sensors. Power management can improve the output performance of TENGs, so TENG-based sensor nodes are typically equipped with a power management system, as illustrated in Fig. 1a. The CMEO strategy defines the maximum energy output limit of TENG per cycle, serving as a significant basis for power management research. The fundamental principle of the CMEO strategy is depicted in Fig. 1b. At the end of the last energy transfer process (Fig. 1b (i)), electrodes A and B are disconnected. At this time, the

potential difference between the two electrodes and the transferred charge are both zero. With the movement of the dielectric layer (Fig. 1b (ii)), the electrodes remain disconnected, and the open-circuit potential difference between the electrodes increases. When the dielectric layer reaches the position shown in Fig. 1b (iii), the potential difference between the two electrodes reaches its maximum. At this point, the two electrodes become conductive, and the charge will be transferred between the two electrodes, achieving maximum transferred charge and potential balance, as shown in Fig. 1b (iv). The energy extracted from the TENG operating in the CMEO mode each cycle can be calculated from the area enclosed by the V-Q diagram in Fig. 1c. Although the CMEO strategy can maximize the output energy of TENG each cycle, significant energy loss can still occur if the load is charged directly. This is due to the mismatch between the TENG's inherent capacitor and the load capacitor. Considering the presence of timing on-switch in the CMEO mode, the mismatch problem can be solved by introducing an inductor to change the energy transfer mode from direct charging to LC oscillation, which is referred to as the CMEO-ULC strategy.

Selecting a superior power management strategy is a prerequisite for developing an efficient passive PMC. To verify the performance of CMEO-ULC power management, the performances of different active power management (i.e. ideal power management) strategies on TENG's capacitive and resistive loads are compared by LTspice simulation software. A freestanding mode TENG with an assumed open circuit voltage of 50 V, a frequency of 10 Hz, and an intrinsic capacitor of 0.5 nF is constructed. As illustrated in Fig. 1d and Fig. 1e, the CMEO-ULC strategy exhibits better performance over other active converter strategies, achieving a 94.2% reduction in charging time and a 39-fold increase in effective power at a 1 MΩ resistor. Therefore, it is feasible and promising to develop a passive PMC based on the CMEO-ULC strategy.

2.2 Topology of the passive CMEO-ULC PMC

The design architecture of the CMEO-ULC PMC is illustrated in Fig. 2a. It comprises a voltage peak detection module and a controlled module, which allows for the activation of the switch following the detection of a voltage peak. Since the

operation of these modules in passive power management is exclusively powered by the energy harvested from the TENG, the design of the circuit structure should be straightforward to reduce extra energy consumption. To this end, a topology of passive CMEO-ULC PMC is constructed in Fig. 2b, where blue and gold areas enable peak detection and switch control, respectively. If the TENG is used to drive electronic devices continuously, the resistor in the dashed line will be introduced. Most low-output TENGs cannot drive electronic devices to work continuously, especially in the era of the IoTs where wireless communications are widely used. Therefore, the subsequent study assumes that a capacitive load is attached to the TENG by default when a resistive load is not specified. The specific working process of this circuit is illustrated in Fig. 2c. When the output voltage of TENG rises, the capacitor C_1 will be charged through the diode D_5 until the output reaches its maximum, as illustrated in Fig. 2c (i). As the output voltage of TENG begins to decrease, the voltage of the PNP base also decreases accordingly. Due to the single conduction of the diode D_5, the potential of the control capacitor C_1 (i.e. the emitter of PNP) remains unchanged. When the potential difference between the emitter and base of PNP reaches the turn-on voltage, the charge stored in C_1 is released, as illustrated in Fig. 2c (ii) and Fig. S1. When the voltage across the resistor $R2$ (i.e. V_{gs}) reaches the threshold voltage V_{th}, the NMOS will be switched on. At this time, the energy stored by the TENG is transferred to the inductor L_1, as illustrated in Fig. 2c (iii). Lastly, the energy stored in L_1 is transferred to C_2 by unidirectional LC oscillation through the diode D_6, as illustrated in Fig. 2c (iv). So far, a complete energy transfer process has been completed.

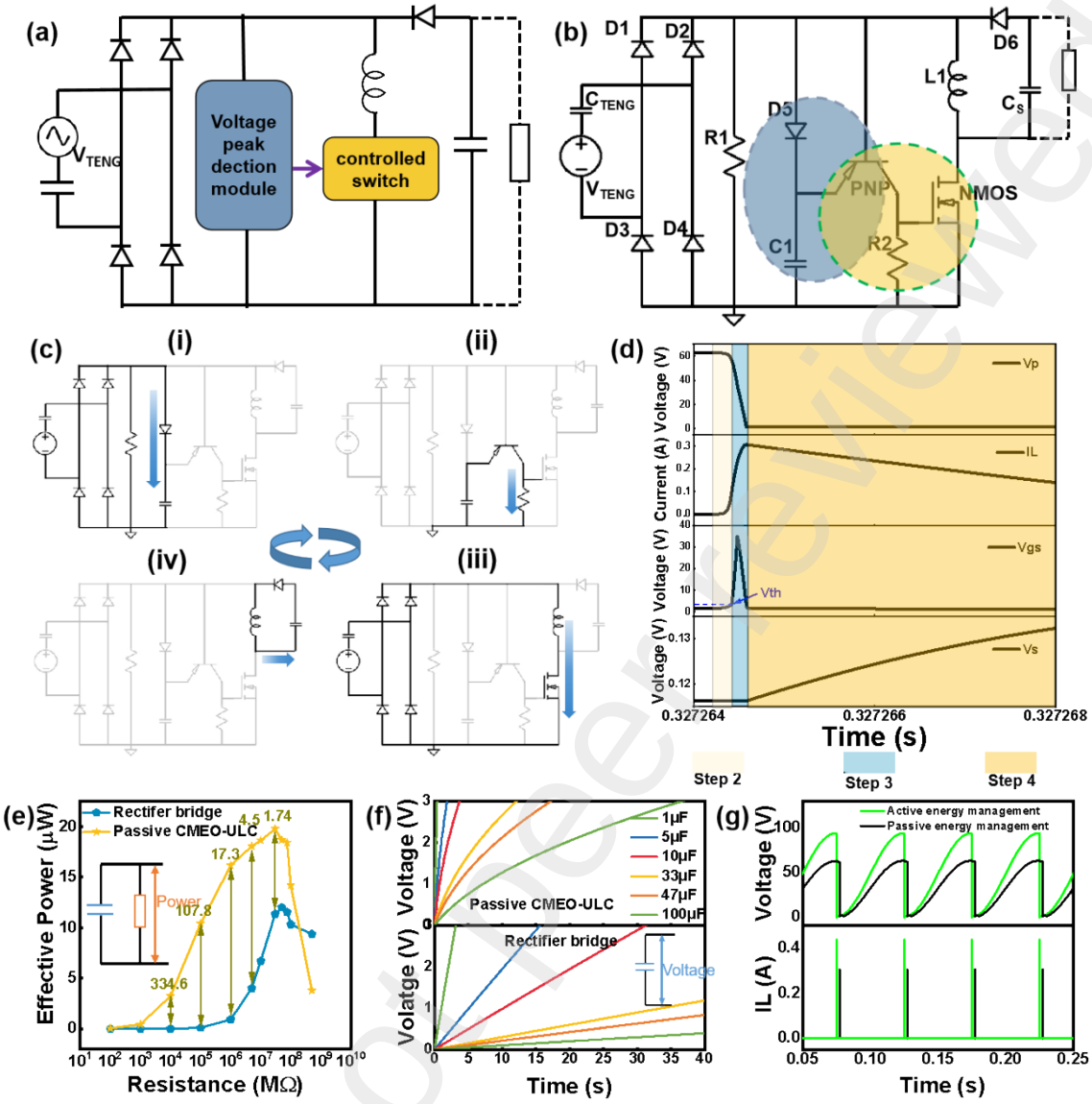

Fig. 2. Working principle of the passive CMEO-ULC PMC. (a) Design architecture, (b) topology, and (c) working process of the passive CMEO-ULC PMC. (d) Waveforms of V_p, I_L, V_g $_s$ and V_s in the process of energy transfer. (e) Comparison of output power, (f) charging performance, and (g) V_p and I_L waveforms between active and passive power management.

To better understand the working process of the passive CMEO-ULC PMC, the TENG constructed in section 2.1 with devices listed in Table S1 is employed to analyze the power management process. Simulated waveforms of V_R $_1$, I_L $_1$, V_g $_s$ and V_s are illustrated in Fig. 2d, providing a clear understanding of the energy transfer process. The PMC can enhance the TENG's

energy harvesting performance effectively. Compared to the rectifier bridge, the effective output of TENG equipped with the PMC increases significantly (Fig. 2e). For a typical resistance of 1 MΩ, the effective output power can be increased by 17.35 times. Moreover, the matching resistance range can be reduced significantly to the actual range of electronic devices. Fig. 2f presents the comparison of charging performance between the PMC and rectifier bridge. For 1 μF, 33 μF and 100 μF capacitors, the charging time decreases by 86.4%, 88.2% and 88.3%, respectively. However, it is worth noting that there exists a certain degree of performance decline in passive power management compared to the standard CMEO-ULC power management (Fig. 1d and e), which is caused by the extra energy consumption of peak detection and controlled switches operation. This is also supported by the decline in port voltage and inductor current (Fig. 2g). To understand the sources and mechanism of energy loss, in-depth research is necessary to be conducted on the process of power management.

2.3 Theoretical Analysis of Energy Transfer Process

Numerical analysis is employed to analyze the energy transfer process. When the NMOS is conducted, the energy stored by the TENG will be transferred to the inductor $L1$ by LC oscillation. Compared to the ideal power management, the overall voltage of TENG in passive power management decreases, which is due to the charge loss of the intrinsic capacitor. In addition, the conduction of the controlled switch (i.e. NMOS) also takes time, which causes the overall voltage of TENG to drop further. Therefore, the power supply voltage is $(1-\theta)\times(1-\alpha)\times V_M$ when LC oscillation occurs，V_M represents the maximum output voltage of TENG，α represents the charge loss coefficient of C_{TENG} caused by the passive power management, and θ represents the delay conduction attenuation coefficient caused by delay conduction of the switch. Besides, given the small value of C_{TENG}, the energy transfer process is notably brief. Consequently, the voltage of TENG during this process can be regarded as approximately unchanged. The differential equation of electrical charge transfer in this

process is expressed as equation (1).

$$L_1\ddot{q} + R_F\dot{q} + \frac{q}{C_T \quad E \quad N \quad G} = (1 - \theta) \times (1 - \alpha) \times V_M$$

(1)

where R_F represents the equivalent resistance. The initial state of the charge transfer process is expressed as equation (2).

$$q(0) = -C_T \quad E \quad N \quad G(1 - \theta) \times (1 - \alpha) \times V_M \text{ and}$$

$$q \quad (\dot{} \quad 0 \quad) = 0,$$

(2)

Therefore, the current of inductor I_L can be derived as equation (3), where ω_I represents the natural angular frequency (equation 4), and Q_I represents the quality factor of the oscillating circuit (equation 5).

$$I_L \quad 1 = \dot{q} = C_T \quad E \quad N \quad GV_M$$

$$(2 - \alpha)(1 - \theta)\frac{\omega_I}{\sqrt{1 - (1/2Q_I)^2}} \times$$

$$s \quad i \quad n\left(\sqrt{1 - \left(\frac{1}{2Q_I}\right)^2}\omega_I t\right)e^{-\frac{\omega_I t}{2Q_I}} \quad (3)$$

$$\omega_I = \frac{1}{\sqrt{L_1 C_T \quad E \quad N \quad G}}$$

(4)

$$Q_I = \frac{1}{R_F}\sqrt{\frac{L_1}{C_T \quad E \quad N \quad G}}$$

(5)

The oscillation period of the RLC oscillation circuit is 2 $\pi\sqrt{L \quad C}$. Since the energy can be transferred from the intrinsic capacitor to the inductor after a 1/4 period, $I_L \quad 1 \quad , \quad m \quad a \quad x$ can be derived with time equal to $\frac{\pi}{2}\sqrt{L \quad C}$, as shown in equation (6). Correspondingly, the maximum energy obtained by the inductor is expressed as equation (7).

$$I_L \quad 1 \quad , \quad m \quad a \quad x = C_T \quad E \quad N \quad GV_M$$

$(2-\alpha)(1-\theta)\frac{\omega_I}{\sqrt{1-(1/2Q_I)^2}}\times$

$s \quad i \quad n\left(\sqrt{1-\left(\frac{1}{2Q_I}\right)^2}\times\frac{\pi}{2}\right)e^{-\frac{\pi}{4Q_I}}$ (6)

$E_L=\frac{1}{2}L_1I_L$, $m \quad a \quad x^2$

(7)

Given that $C_T \quad E \quad N \quad G$ is generally in several nFs, the quality factor Q will be large, while $\frac{1}{2Q_I}$ is nearly zero. Therefore, the energy E_L acquired by the inductor can be approximated as $\frac{1}{2}(1-\theta)^2(2-\alpha)^2$ $C_T \quad E \quad N \quad {}_GV_M{}^2e^{-\frac{\pi}{2Q_I}}$, from which it can be found that E_L is mainly related to the accumulated charge loss coefficient and delay conduction coefficient.

Subsequently, the energy acquired by $L1$ is transferred to the energy storage capacitor C_s via LC oscillation. Given the large value of C_s, $V_c \quad {}_s$ can be assumed to remain unchanged during a single charge transfer process. Then, the differential equation of the electrical charge transfer is expressed as equation (8).

$L_1\ddot{q}+R_S\dot{q}+V_c \quad s$

$=0$

(8)

where R_S represents the equivalent resistance of the secondary energy transfer loop. With the initial condition $q \quad (\quad 0 \quad) =$ $I_L \quad 1 \quad , \quad m \quad a \quad x$ and $q(0)=0$, the current $I_L \quad {}_2$ can be derived as equation (9).

$I_L \quad {}_2=\dot{q}=e^{-\frac{R_S}{L_1}t}$

$\left(I_m \quad a \quad x+\frac{V_c \quad {}_s}{L_1}e^{-\frac{R_S}{L_1}t}\right)-\frac{V_c \quad {}_s}{R_S}$

(9)

When I_L $_2$ drops to zero, the process of C_s being charged ends. Therefore, the duration t_2 can be derived as equation (10). Correspondingly, the energy acquired by C_s can be expressed as equation (11).

$t_2 = \frac{L}{R_S} l$ $n\left(1 + \frac{R_S I_m}{V_c}\right)$

(10)

$E = \int_0^{t_2} V_c$ $_s \dot{q} d$ $t =$ $\frac{LV_c}{R_S}$ $\left(I_m\right.$ $\left. - \frac{V_c}{L} t_2\right)$

(11)

Through the above numerical analysis, the energy loss of the PMC can be identified as delay conduction loss, the accumulated charge loss and the secondary oscillating loop impedance loss.

3. Performance analysis of the device selection

Power management performance can be improved by reducing energy losses, which originate from topology and electronic devices. Since the topology of the circuit is predetermined and simplified, device selection becomes a crucial factor for reducing energy loss. Fig. S2 shows the charging performance comparison of PMCs faced with different combinations of device selection and output amplitudes by simulation. The specific device selections are detailed in Table S1, and the simulated voltage output of TENG varies from 10 V to 60 V. It is evident that different device combinations lead to significant differences in the energy harvesting performance, especially when the TENG's output is low. Therefore, to ensure the normal operation of the PMC, it is crucial to study the impact of devices on the power management performance. Since the types of energy losses are specified in section 2.3, this makes the subsequent impact study on electronic devices explicit. Fig. 3a illustrates the Schematic illustration of V_R $_1$ caused by different types of energy losses, which can assist in identifying the energy loss source. The devices are divided into basic components and switching components according to their characteristics. The impact

of devices on the power management performance is explored by the control variable method. Optional devices are listed in Table S2. For the convenience of subsequent comparative research, the PMC with R 1-500MΩ, C 1-0.2 n F, $L1$-22μH, R 2-20MΩ, PNP-mmbt3906, and NMOS-2N7002 is set as the reference circuit. Since transient changes of circuit nodes are difficult to capture experimentally, LTspice simulation software is employed for research. To ensure the reliability of the analysis, the simulation inferences need to be further validated experimentally. In this study, the TENG-embedded cylindrical roller bearing (TCRB) proposed in [37] is introduced as an experimental object, and its equivalent power supply is constructed, as shown in Fig. 3b. The electronic devices listed in Table S2 are also purchased for experimental verification. Last, the fabricated selectable-device PMC and experiment setup are presented in Fig. S3 and S4.

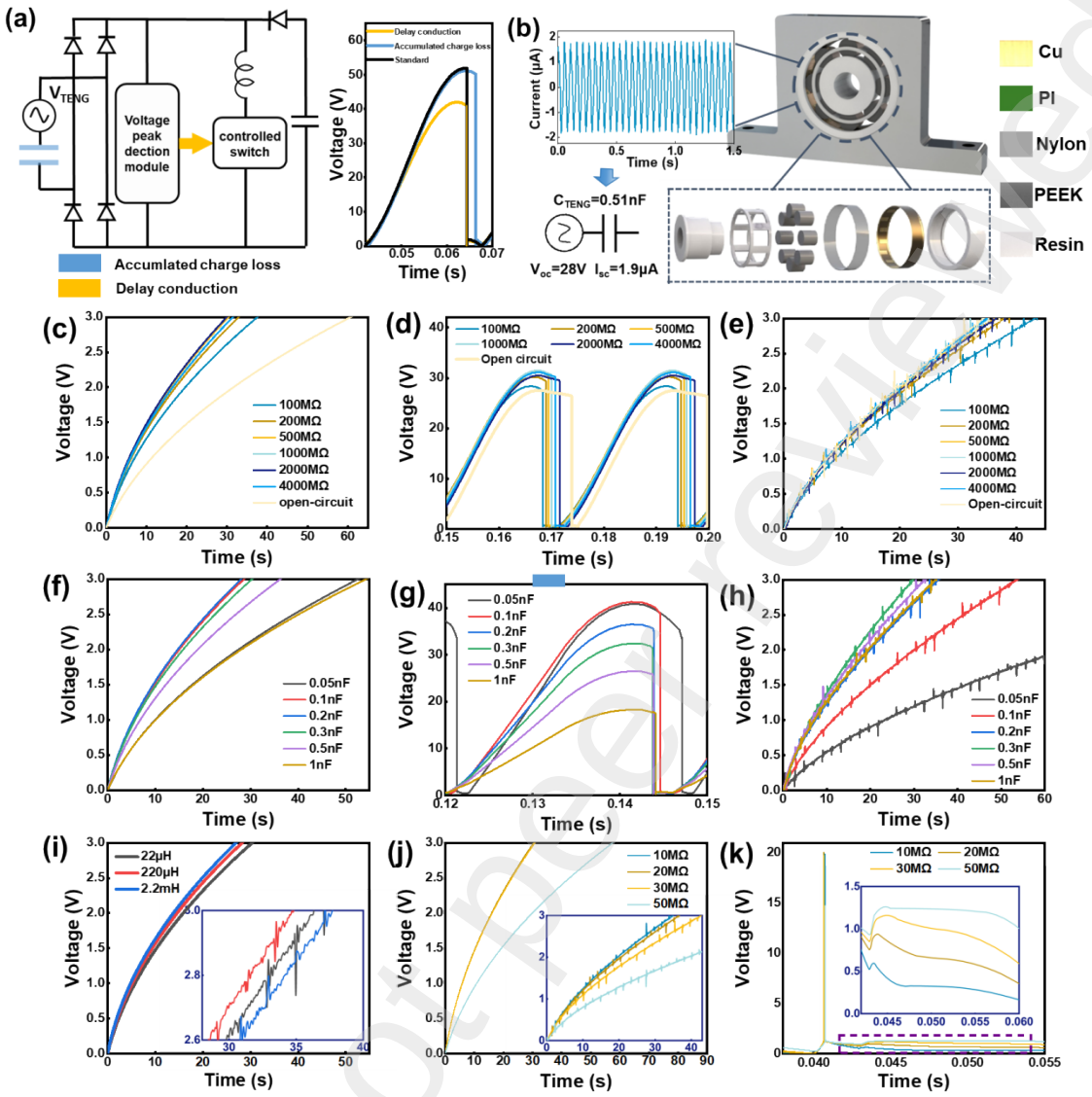

Fig. 3. Impact analysis of basic devices. (a) Schematic illustration of V_{R_1} caused by different energy losses. (b) Equivalent power supply model of the TCRB [37]. (c) Simulation waveforms of charging performance, and (d) V_{R_1} with different resistor R_1. (e) Experimental charging performance with different resistor R_1. (f) Simulation waveforms of charging performance, and (g) V_{R_1} with different capacitor C_1. (h) Experimental charging performance with different capacitor C_1. (i) Charging performance with different inductor

L 1. (j) Charging performance with different resistor R 2. (k) Simulation waveform of V_g $_s$ with different resistor R 2.

3.1 Impact analysis of basic devices

The function of the resistor R 1 is to provide a current loop when NMOS is switched off, ensuring that the voltage of the PNP base can track the TENG's output. This mechanism allows V_b $_e$ to reach the turn-on voltage of the PNP when the TENG's output drops. Notably, the resistance of R 1 should be relatively large to ensure that the poles of TENG are approximately disconnected. Fig. 3c presents the charging performance of TENG using PMCs with different R 1 by simulation. It can be observed that R 1 with either excessively large or small value will result in a longer charging time. The reason for this can be further explored by examining the waveform of V_R $_1$ (Fig. 3d). When the resistance of R 1 is small, the accumulated charge on C_T $_E$ $_N$ $_G$ will be lost through R 1. Conversely, R 1 with excessively large resistance will prevent the base of PNP from tracking the output, making it difficult to detect the peak output accurately. Correspondingly, resistors with identical values in the simulation are employed to test the charging performances by experiment, as illustrated in Fig. 3e. Unlike the simulation results, there is no significant difference in the time taken for the energy storage capacitor to be charged when R 1 is greater than 500 MΩ.This discrepancy is possibly due to the large leakage current of PNP and NMOS in practice, which allows the base of PNP to change with the TENG's output even if there is no

branch of R 1.

The function of the capacitor C 1 is to provide energy for conducting NMOS and realize the detection of the peak output in conjunction with the diode D 5. Fig. 3f presents the charging performance of TENGs using PMCs with different C 1 by simulation. Obviously, a capacitance value that is either excessively large or small will adversely affect the charging performance. The reason for this can be further explored by examining the waveform of V_R 1 (Fig. 3g). A larger capacitance will lead to a decrease in the peak of V_R 1, indicating a reduction in the accumulated charge in C_T E N G. While a small capacitance does not reduce the accumulated charge in C_T E N G, limited stored energy in C 1 will delay the conduction of NMOS, which will also deteriorate the power management performance. Correspondingly, the charging performances of TENGs using PMCs with identical capacitors used in the simulation are tested experimentally, as illustrated in Fig. 3h. Consistent with the simulation results, excessive or insufficient capacitance values will lead to a decline in the power management performance.

The function of inductor $L1$ is to extract the energy stored in TENG and transfer energy to capacitor C_s via LC oscillation. Fig. 3i illustrates the charging performance of TENGs using PMCs with different inductor $L1$ by simulation. Evidently, with the increase of inductance, the charging time decreases correspondingly. However, the experimental result (the insert of Fig. 3i) indicates that the optimal charging performance is achieved using a PMC with 220 μ H inductor. This discrepancy may be attributed to that the idealized inductor model used in the simulation does not account for the existence of magnetic loss and inherent resistance. Each power management cycle encompasses two LC oscillation processes.

The quality factor of a damped LC oscillator circuit, denoted as $Q = \frac{1}{r}\sqrt{\frac{L}{C}}$, quantifies the energy loss in the energy transfer process. Since C_{TENG} is very small, the resistance of inductor $L1$ exerts negligible impact on Q in the initial LC oscillation process. However, given the close order of magnitude of C_s and $L1$, the resistance of the inductor will significantly impact Q of the second LC oscillation process, which is consistent with the energy loss analyzed in section 2.3. By setting an appropriate equivalent resistance of inductor $L1$, the simulation results of charging performance can align with the experimental results, as illustrated in Fig. S5. Therefore, the above analysis shows that the inductor with small impedance should be selected.

The resistor $R2$ serves to establish V_{gs}, thereby enabling the NMOS to conduct. Fig. 3j presents the charging performance of TENGs using PMCs with different resistor $R2$ by simulation, and the experimental result (see the insert of Fig. 3j) aligns with the simulation results. The charging performance of TENGs remains relatively stable when the resistance ranges from 10 MΩ and 30 MΩ. However, the charging performance declines when the resistance reaches 50 MΩ. Conducting NMOS requires the equivalent gate capacitor to be charged up to V_{th}, while switching off NMOS necessitates the discharge of the charge. Excessive resistance prevents the discharge of charges, making it difficult for the NMOS to shut down completely, as illustrated in Fig. 3k. This will cause a large leakage current through the NMOS (Fig. S6), increasing accumulated charge loss.

3.2 Impact analysis of switching devices

Switching devices are essential for power management control. The PNP transistor implements the peak checking function together with the control capacitor and determines the energy release of the control capacitor. The NMOS transistor acts as the main switch for the TENG's CMEO strategy. Different from basic devices, switching devices involve many physical parameters, so the impact mechanism of the devices on

the power management performance is not straightforward. A deep understanding of the physical characteristics of switching devices can contribute to the impact analysis of switching devices.

With the help of the equivalent model of PNP (Fig. 4a), the changes occurring inside the PNP during the process of power management can be revealed. C_j and C_d denote barrier capacitance and diffusion capacitance respectively, and are collectively referred to as junction capacitance. Upon the completion of the previous energy transfer cycle, both the control capacitor and junction capacitor will be charged as the output voltage of TENG rises, causing an increased accumulated charge loss. Consequently, the PNP with a small emitter junction capacitance should be selected. To corroborate the above inference, five distinct types of PNP are selected, and their capacitance values are presented in Table S3. Fig. 4b shows the charging performance of TENGs using PMCs with different PNPs by experiment. Evidently, the energy harvesting performances of the PMC with mmbt5401 and mmbt3906 are superior, while the energy harvesting performance significantly deteriorates when 2SA2056 is selected. This trend generally aligns with the changes in junction capacitance of PNP. This inference can be further validated by the waveform of V_{R1}, as illustrated in Fig. 4c. It can be observed that the V_{R1} peak value of 2SA2056 decays, which is due to larger energy loss in C_{TENG} caused by the junction capacitor.

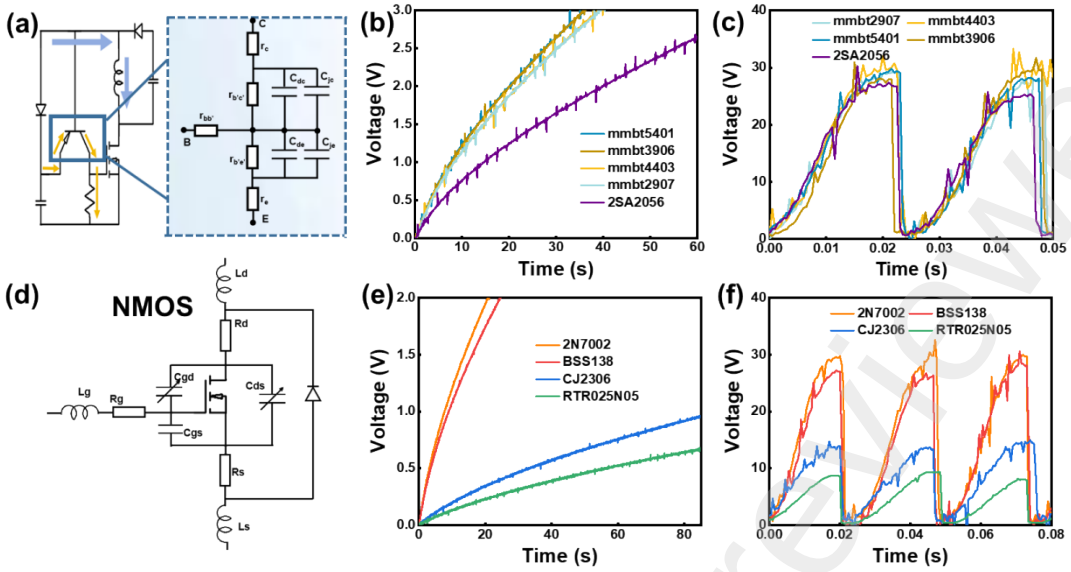

Fig. 4. Impact analysis of switching devices. (a) Schematic illustration of the equivalent model of PNP. (b) Charging performance, and (c) V_{R1} waveform with different PNPs by experiment. (d) Schematic illustration of the equivalent model of NMOS. (e) Charging performance, and (f) V_{R1} waveform with different NMOSs by experiment.

To study the influence of NMOS on the power management performance, an equivalent model of NMOS that considers capacitor effects is introduced, as illustrated in Fig. 4d. There are equivalent capacitors between each terminal of NMOS, named C_{gd}, C_{gs} and C_{ds}. As the output voltage of TENG rises, both C_{ds} and C_{gd} will be charged, causing an increased charge loss. Besides, to ensure the conduction of NMOS, C_{gs} must be charged to V_{th}. Therefore, reducing parasitic capacitance can contribute to the efficient operation of the PMC. To verify the impact of parasitic capacitors on power management performance, four different NMOSs are employed. Their specific capacitance parameters are listed in Table S4. As illustrated in Fig. 4e, the charging performance of TENG using the PMC with 2N7002 exhibits the best, obviously superior to those with CJ2306 and RTR025N05. This trend aligns with the change in parasitic capacitance of the NMOS. Moreover, the

V_R $_1$ waveform in Fig. 4f illustrates from another perspective that the NMOS with a larger parasitic capacitance will increase accumulated charge loss. Compared with PNP, NMOS has a more significant impact on the power management performance. This is primarily because the variation in parasitic capacitance of NMOS with identical package is usually greater than that in junction capacitance of PNP. Last, it is worth noting that other physical parameters of NMOS, such as gate threshold voltage (V_t $_h$) and zero gate voltage drain current (I_D $_S$ $_S$) theoretically affect the power management performance. A low V_t $_h$ can conduct NMOS faster, thereby reducing the delayed conduction loss, while a low leakage current can reduce the accumulated charge loss. However, since differences in I_D $_S$ $_S$ and V_t $_h$ of identical package are usually small, the parasitic capacitance becomes the dominant factor affecting the performance of the PMC.

4. Demonstration

Fig. 5a presents a prototype of the fabricated PMC with optimized device selection, whose devices used are C 1-0.33 n F , $L1$-220μH, R 2-20MΩ, PNP-mmbt3906, and NMOS-2N7002. The size of PMC is comparable to that of a RMB 1 coin, making it easy to integrate with various TENGs. Qualified PMCs should be adapted to different output frequencies, so the performances of the PMC at different speeds are tested. As illustrated in Fig. 5b, the charging performance of the TENG improves at different speeds, but decreases as the frequency decreases. This is because the output amplitude of the TENG is small at low rotational speed, increasing the proportion of energy loss to available energy. Fig. 5c shows the TENG's output power connected to different resistors with the PMC. Similar to the simulation results, the PMC can reduce the matching load resistance of TENG, and the output power of a 1 MΩ can be increased by 3.48 times. The reason why the experimental results are inferior to the simulation results may be that the energy consumed by conducting NMOS is more than expected

and the intrinsic capacitor of TENG is smaller than the value constructed in the model. The performance of the PMC on a capacitive load is demonstrated with a TENG-based wireless temperature sensing system. As shown in Fig. 5d, the PMC and wireless sensor are mounted above the bearing seat. When the 1000 μF capacitor is charged to 4V, the energy will be released to drive the sensor. Previously, the TENG with the rectifier bridge takes 45 minutes to charge the capacitor, while it only takes 17 minutes with the PMC. With the help of the circuit, 62% of the charging time is saved. Furthermore, the effectiveness of the PMC applied to a contact separation mode TENG is demonstrated. As illustrated in Fig. 5e, a 47 μF capacitor can be charged to 0.98 V by manually tapping 200 times with the PMC, while only 0.16V is charged by the rectifier bridge. Last, the performance of PMC is also verified by a TENG for vibration energy harvesting, whose structure can be found in [38]. As illustrated in Fig. 5f, 61.7% of charging time is saved compared to the rectifier bridge.

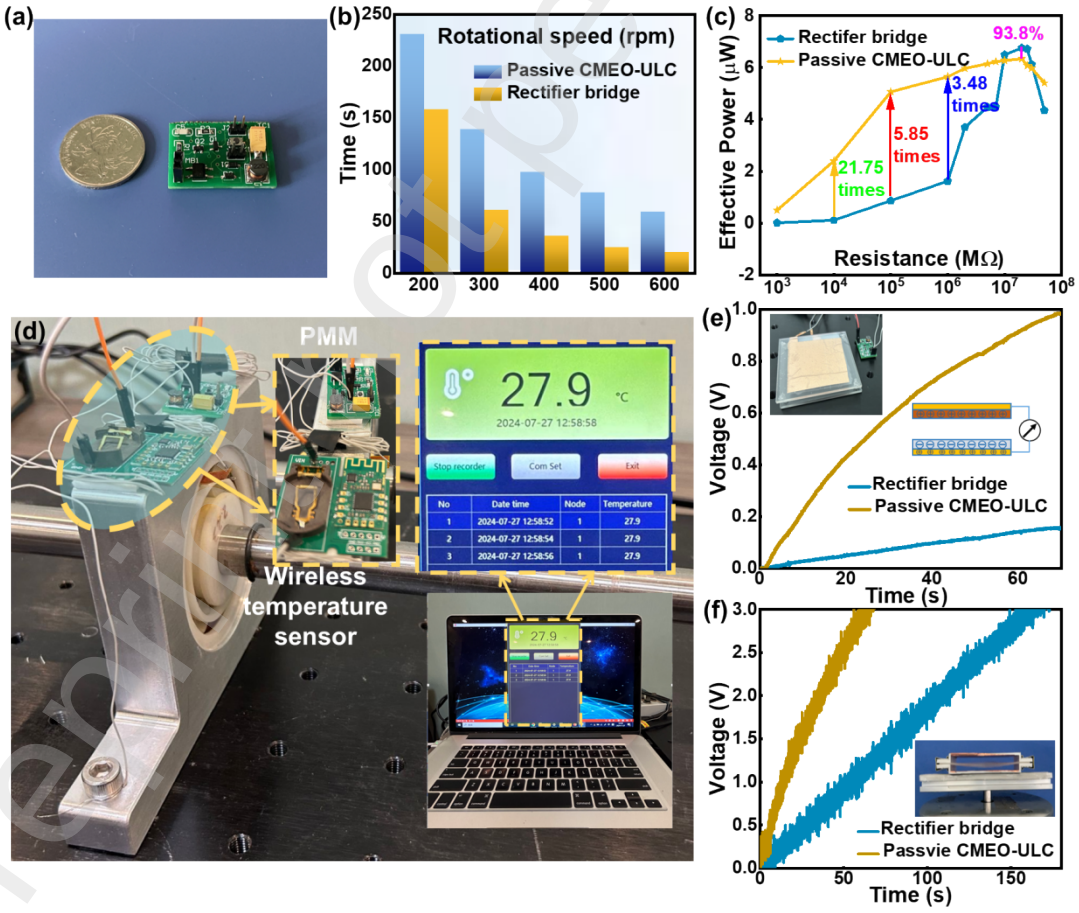

Fig. 5. Demonstration of the passive CMEO-ULC PMC. (a) Prototype of the PMC. (b)

Charging performance of the PMC at different speeds. (c) Experimental output power of the TCRB with the PMC. (d) Wireless communication demonstration of TENG-based sensor node through the PMC. (e) Charging performance comparison of a contact-separation mode TENG, and (f) a TENG for vibration energy harvesting with the PMC and the rectifier bridge [38].

5. Conclusion

In conclusion, this study introduces a self-driven PMC that integrates the CMEO strategy and unidirectional LC oscillation. The topology and operating principle of the PMC are depicted in detail. For a typical freestanding TENG, the simulation results show that PMC can help the TENG shorten the charging time to a 47 μF capacitor by 88.3%, and increase its output power of a 1 MΩ load by 17.35 times. Due to the weak output and small intrinsic capacitance of TENGs, the performance of the PMC is susceptible to device selection in practice. Therefore, the impact of semiconductor devices on power management performance is investigated systematically. By establishing the numerical equation of energy transfer, energy loss sources are first qualitatively identified as accumulated charge loss, conduction delay loss and oscillating loop impedance loss. Then, the correlation of these energy losses with device selection is analyzed by simulation and experiment. With optimized device selection, the fabricated PMC can successfully reduce a 6.7 μW-output TENG's charging time to a 47 μF capacitor by 62.8%, and increase the output power at a 1 MΩ by 3.48 times. Moreover, the PMC also exhibits good universality to various TENGs. Overall, the proposed PMC can improve the performance of TNEG-based sensor nodes greatly, which is of great significance for promoting the application of TENGs.

Declaration of competing interest

The authors declare that they have no known competing financial interests or personal relationships that could have appeared to influence the work reported in this paper.

Data availability

Data will be made available on request.

Acknowledgements

The work was supported by the Application Research Program of Liaoning Province (Grant No. 2022JH2/01300219), Dalian Outstanding Young Scientific and Technological Talents Project (2021RJ11), and the Fundamental Research Funds for the Central Universities (Grant No. 3132024210).

Reference

[1] F.-R. Fan, Z.-Q. Tian, Z. Lin Wang, Flexible triboelectric generator, Nano Energy 1 (2012) 328-334. https://doi.org/10.1016/j.nanoen.2012.01.004

[2] S. Sripadmanabhan Indira, C. Aravind Vaithilingam, K.S.P. Oruganti, F. Mohd, S. Rahman, Nanogenerators as a Sustainable Power Source: State of Art, Applications, and Challenges, Nanomaterials 9 (2019). https://doi.org/10.3390/nano9050773

[3] Z.L. Wang, J. Chen, L. Lin, Progress in triboelectric nanogenerators as a new energy technology and self-powered sensors, Energy & Environmental Science 8 (2015) 2250-2282. https://doi.org/10.1039/c5ee01532d

[4] B. Chen, Y. Yang, Z.L. Wang, Scavenging Wind Energy by Triboelectric Nanogenerators, Advanced Energy Materials 8 (2018). https://doi.org/10.1002/aenm.201702649

[5] C. Wu, A.C. Wang, W. Ding, H. Guo, Z.L. Wang, Triboelectric Nanogenerator: A Foundation of the Energy for the New Era, Advanced Energy Materials 9 (2018). https://doi.org/10.1002/aenm.201802906

[6] M. Xu, T. Zhao, C. Wang, S.L. Zhang, Z. Li, X. Pan, et al., High Power Density Tower-like Triboelectric Nanogenerator for Harvesting Arbitrary Directional Water Wave Energy, ACS Nano (2019). https://doi.org/10.1021/acsnano.8b08274

[7] S.L. Zhang, M. Xu, C. Zhang, Y.-C. Wang, H. Zou, X. He, et al., Rationally designed sea snake structure based triboelectric nanogenerators for effectively and efficiently harvesting ocean wave energy with minimized water screening effect, Nano Energy 48 (2018) 421-429. https://doi.org/10.1016/j.nanoen.2018.03.062

[8] L. Xu, T. Jiang, P. Lin, J.J. Shao, C. He, W. Zhong, et al., Coupled Triboelectric Nanogenerator Networks for Efficient Water Wave Energy Harvesting, ACS Nano 12 (2018) 1849-1858. https://doi.org/10.1021/acsnano.7b08674

[9] C. Rodrigues, D. Nunes, D. Clemente, N. Mathias, J.M. Correia, P. Rosa-Santos, et al., Emerging triboelectric nanogenerators for ocean wave energy harvesting: state of the art and future perspectives, Energy & Environmental Science 13 (2020) 2657-2683. https://doi.org/10.1039/d0ee01258k

[10] J. Chen, G. Zhu, W. Yang, Q. Jing, P. Bai, Y. Yang, et al., Harmonic-Resonator-Based Triboelectric Nanogenerator as a Sustainable Power Source and a Self-Powered Active Vibration Sensor, Advanced Materials 25 (2013) 6094-6099. https://doi.org/10.1002/adma.201302397

[11] H. Yu, Z. Xi, H. Du, H. Yang, Z. Qian, X. Guo, et al., High Performance and Stackable Trampoline Like-Triboelectric Vibration Energy Harvester for In-Situ Powering Sensor Node with Data Wirelessly Transmitted Over 1000-m, Advanced Energy Materials (2024). https://doi.org/10.1002/aenm.202400585

[12] Z. Liu, C. Zhao, G. Hu, Y. Yang, A multi-degree-of-freedom triboelectric energy harvester for dual-frequency vibration energy harvesting, Mechanical Systems and Signal Processing 188 (2023). https://doi.org/10.1016/j.ymssp.2022.109951

[13] T. Du, X. Zuo, F. Dong, S. Li, A.E. Mtui, Y. Zou, et al., A Self-Powered and Highly Accurate Vibration Sensor Based on Bouncing-Ball Triboelectric Nanogenerator for Intelligent Ship Machinery Monitoring, Micromachines 12 (2021). https://doi.org/10.3390/mi12020218

[14] H. Yuan, H. Yu, X. Liu, H. Zhao, Y. Zhang, Z. Xi, et al., A High-Performance Coniform Helmholtz Resonator-Based Triboelectric Nanogenerator for Acoustic Energy Harvesting, Nanomaterials 11 (2021). https://doi.org/10.3390/nano11123431
[15] J. Yang, J. Chen, Y. Liu, W. Yang, Y. Su, Z.L. Wang, Triboelectrification-Based Organic Film Nanogenerator for Acoustic Energy Harvesting and Self-Powered Active Acoustic Sensing, ACS Nano 8 (2014) 2649-2657. https://doi.org/10.1021/nn4063616
[16] Y. Li, C. Liu, S. Hu, P. Sun, L. Fang, S. Lazarouk, et al., Self-Powered Acoustic Sensor Based on Triboelectric Nanogenerator for Smart Monitoring, Acoustics Australia 50 (2022) 383-391. https://doi.org/10.1007/s40857-022-00275-4
[17] M. Yuan, C. Li, H. Liu, Q. Xu, Y. Xie, A 3D-printed acoustic triboelectric nanogenerator for quarter-wavelength acoustic energy harvesting and self-powered edge sensing, Nano Energy 85 (2021). https://doi.org/10.1016/j.nanoen.2021.105962
[18] Y. Huang, T. Du, C. Xiang, Y. Zhang, J. Si, H. Yu, et al., Research Progress of Acoustic Energy Harvesters Based on Nanogenerators, International Journal of Energy Research 2023 (2023) 1-40. https://doi.org/10.1155/2023/5568046
[19] T. Zhou, C. Zhang, C.B. Han, F.R. Fan, W. Tang, Z.L. Wang, Woven Structured Triboelectric Nanogenerator for Wearable Devices, ACS Applied Materials & Interfaces 6 (2014) 14695-14701. https://doi.org/10.1021/am504110u
[20] Z. Qin, Y. Yin, W. Zhang, C. Li, K. Pan, Wearable and Stretchable Triboelectric Nanogenerator Based on Crumpled Nanofibrous Membranes, ACS Applied Materials & Interfaces 11 (2019) 12452-12459. https://doi.org/10.1021/acsami.8b21487
[21] D. Tan, B. Xu, Y. Gao, Y. Tang, Y. Liu, Y. Yang, et al., Breathable fabric-based triboelectric nanogenerators with open-porous architected polydimethylsiloxane coating for wearable applications, Nano Energy 104 (2022). https://doi.org/10.1016/j.nanoen.2022.107873
[22] S. Niu, Z.L. Wang, Theoretical systems of triboelectric nanogenerators, Nano Energy 14 (2015) 161-192. https://doi.org/10.1016/j.nanoen.2014.11.034
[23] Y. Zhou, P. Zhang, J. Li, X. Mao, Recent progress of triboelectric nanogenerator-based power management and information processing circuit, Materials Today Sustainability 23 (2023). https://doi.org/10.1016/j.mtsust.2023.100426
[24] S. Xu, L. Zhang, W. Ding, H. Guo, X. Wang, Z.L. Wang, Self-doubled-rectification of triboelectric nanogenerator, Nano Energy 66 (2019). https://doi.org/10.1016/j.nanoen.2019.104165
[25] A. Ghaffarinejad, J. Yavand Hasani, D. Galayko, P. Basset, Superior performance of half-wave to full-wave rectifier as a power conditioning circuit for triboelectric nanogenerators: Application to contact-separation and sliding mode TENG, Nano Energy 66 (2019). https://doi.org/10.1016/j.nanoen.2019.104137
[26] W. Peng, S. Du, The Advances in Conversion Techniques in Triboelectric Energy Harvesting: A Review, IEEE Transactions on Circuits and Systems I: Regular Papers 70 (2023) 3049-3062. https://doi.org/10.1109/tcsi.2023.3261780
[27] S. Xu, W. Ding, H. Guo, X. Wang, Z.L. Wang, Boost the Performance of Triboelectric Nanogenerators through Circuit Oscillation, Advanced Energy Materials 9 (2019). https://doi.org/10.1002/aenm.201900772

[28] X. Cheng, W. Tang, Y. Song, H. Chen, H. Zhang, Z.L. Wang, Power management and effective energy storage of pulsed output from triboelectric nanogenerator, Nano Energy 61 (2019) 517-532. https://doi.org/10.1016/j.nanoen.2019.04.096
[29] S. Niu, X. Wang, F. Yi, Y.S. Zhou, Z.L. Wang, A universal self-charging system driven by random biomechanical energy for sustainable operation of mobile electronics, Nature Communications 6 (2015). https://doi.org/10.1038/ncomms9975
[30] H. Zhang, D. Galayko, P. Basset, General analysis and optimization of a two-stage power management circuit for electrostatic/triboelectric nanogenerators, Nano Energy 103 (2022). https://doi.org/10.1016/j.nanoen.2022.107816
[31] Y. Zi, S. Niu, J. Wang, Z. Wen, W. Tang, Z.L. Wang, Standards and figure-of-merits for quantifying the performance of triboelectric nanogenerators, Nature Communications 6 (2015). https://doi.org/10.1038/ncomms9376
[32] X. Cheng, L. Miao, Y. Song, Z. Su, H. Chen, X. Chen, et al., High efficiency power management and charge boosting strategy for a triboelectric nanogenerator, Nano Energy 38 (2017) 438-446. https://doi.org/10.1016/j.nanoen.2017.05.063
[33] F. Xi, Y. Pang, W. Li, T. Jiang, L. Zhang, T. Guo, et al., Universal power management strategy for triboelectric nanogenerator, Nano Energy 37 (2017) 168-176. https://doi.org/10.1016/j.nanoen.2017.05.027
[34] H. Qin, G. Gu, W. Shang, H. Luo, W. Zhang, P. Cui, et al., A universal and passive power management circuit with high efficiency for pulsed triboelectric nanogenerator, Nano Energy 68 (2020). https://doi.org/10.1016/j.nanoen.2019.104372
[35] H. Qin, G. Cheng, Y. Zi, G. Gu, B. Zhang, W. Shang, et al., High Energy Storage Efficiency Triboelectric Nanogenerators with Unidirectional Switches and Passive Power Management Circuits, Advanced Functional Materials 28 (2018). https://doi.org/10.1002/adfm.201805216
[36] W. Harmon, D. Bamgboje, H. Guo, T. Hu, Z.L. Wang, Self-driven power management system for triboelectric nanogenerators, Nano Energy 71 (2020). https://doi.org/10.1016/j.nanoen.2020.104642
[37] Y. Xin, T. Du, T. Liu, P. Sun, M. Zhu, L. Zheng, et al., Triboelectric nanogenerator embedded cylindrical roller bearing for rotational energy harvesting and self-powered fault diagnosis, Sensors and Actuators A: Physical 362 (2023) 114664. https://doi.org/https://doi.org/10.1016/j.sna.2023.114664
[38] T. Du, D. Shen, Z. Xi, H. Yu, F. Dong, C. Zhao, et al., Highly adaptive and broadband triboelectric energy harvester with stretching silicone rubber strip for variable harmonic frequency vibration, Nano Research 17 (2024) 4089-4099. https://doi.org/10.1007/s12274-023-6309-3